Proton Diffusion in Strontium Cerate Ceramics studied by Quasielastic Neutron Scattering and Impedance Spectroscopy

Ch. Karmonik[a], R. Hempelmann[a], Th. Matzke[b], and T. Springer[b]

[a] Physikalische Chemie, Universität des Saarlandes, 66123 Saarbrücken, Germany
[b] Forschungszentrum Jülich, 52425 Jülich, Germany

Z. Naturforsch. **50a**, 539–548 (1995); received November 11, 1994

Dedicated to Prof. Dr. Dr. h.c. mult. E. Wicke on the occasion of his 80th birthday

Perovskite structured strontium cerate doped with ytterbium and water, e.g. $SrCe_{0.95}Yb_{0.05}H_{0.02}O_{2.985}$, is a well known proton conductor at elevated temperatures. We have studied its proton conductivity or diffusivity, respectively, by impedance spectroscopy, IS, and by quasielastic neutron scattering, QENS. While the former method yields a macroscopic proton diffusion coefficient, the latter method allows to elucidate the microscopic proton diffusion mechanism. It consists of a sequence of free diffusion and trapping/escape events with the Yb^{3+} ions acting as trapping centers. The self-diffusion coefficient obtained with QENS agrees with the conductivity diffusion coefficient obtained with IS.

1. Introduction

Many oxides dissolve – frequently inadvertently – small amounts of water and become proton conducting at elevated temperatures [1]. Larger amounts of water – up to several mol% – can be dissolved in some aliovalently doped perovskites like $SrCeO_3$ doped with Yb_2O_3 [2], $BaCeO_3$ doped with Nd_2O_3 [3], or $SrZrO_2$ doped with Y_2O_3 [4]. In these systems, the threevalent dopant substitutes a Ce^{4+} or Zr^{4+} ion; the charge deficiency is balanced either by vacancies in the oxygen sublattice (without water) or by protons on interstitial sites (with water) forming a covalent bond to one of the adjacent O^{2-} ions. These proton conducting oxides can be used as solid electrolytes in a number of electrochemical devices at high temperatures [5]; for the measurement of the hydrogen activity in molten aluminium in the casting process, a galvanic cell type hydrogen sensor has been commercialized by a Japanese company using $CaZrInO_3$ ceramics developed by Iwahara et al. [6].

Solide oxide fuel cells (SOFC) at the present state of technology use oxygen conducting yttrium stabilized zirconia as solid electrolyte. In order to achieve sufficient conductivity an operating temperature of about 1000 °C is necessary. This is very inconvenient because all interconnector and construction materials have to consist of ceramics with their well-known problems of brittleness. Therefore a short-term objective of development is a reduction of the operating temperature to 800 °C or lower; in this respect proton conducting oxides are promising candidates for the solid electrolyte and could help to realize the development of large-scale power plants on SOFC basis, where fossile fuel is directly converted into electricity.

The essential physical property of the solid electrolyte is its ionic conductivity, which is related to its ionic diffusivity (Nernst-Einstein-Relation). Macroscopic proton conductivity studies are numerous [1]; for a microscopic investigaion of the proton diffusion, incoherent quasieleastic neutron scattering (QENS) is a particularly powerful method because it allows to study the diffusion process on microscopic scales of time and space simultaneously. For our study of the proton diffusion mechanism in a proton conducting oxide [7] we have chosen Yb-doped $SrCeO_3$ for several reasons:

i) Yb-doped $SrCeO_3$ in moist atmosphere is proton conducting in the temperature range 400 °C to 1000 °C with increasing electronic contributions at the more elevated temperatures but without any measurable contribution of oxygen ions to the total conductivity under these conditions [8]. This is favourable because a diffusing oxygen ion could carry a proton, thus forming hydroxide ion, and could thus act as vehicle.

Reprint requests to Prof. R. Hempelmann.

0932-0784 / 95 / 0600-0539 $ 06.00 © – Verlag der Zeitschrift für Naturforschung, D-72027 Tübingen

ii) Since according to the Nernst-Einstein-Relation conductivity is the product of concentration and diffusion coefficient, large proton conductivity means (relatively) large proton concentration and/or (relatively) large proton diffusion coefficient. Both properties are desirable for a quasielastic neutron scattering experiment in order to obtain sufficient scattering intensity and sufficient energetical broadening of the elastic line, respectively.

iii) The proton content of several mol% of Yb-doped $SrCeO_3$, although large in comparison to other proton conducting oxides, is still to be considered as small for a quasielastic neutron scattering experiment. Therefore it is important that the main constituents Sr, Ce, and O exhibit hardly any incoherent neutron scattering cross section so that in spite of their low concentration the protons with their huge cross section are the dominant scatterers.

As already mentioned, in Yb-doped $SrCeO_3$ the Yb^{3+} ions substitute Ce^{4+} ions and thus carry an effective negative charge. This negative charge attracts protons; differences in proton site energies actually are evident from the model independent evaluation of our neutron scattering data to be described in Sect. 4.1; the tentative results thus obtained encouraged us to perform the final data evaluation, Sect. 4.2, in the framework of the so-called two-state-model which will be explained in Section 2. In Sect. 4.3 we report on our macroscopic electrochemical measurements, which were performed on the same sample batch like the neutron scattering experiment. The results are discussed and compared in Sect. 5; the agreement between the macroscopically obtained proton diffusion coefficient and the microscopically determined proton self-diffusion coefficient is striking and thus supports and confirms our conclusions.

2. Quasielastic Neutron Scattering and the Two-State-Model

The quasielastic neutron scattering method [9, 10] makes use of the slightly inelastic scattering at Q values (scattering angles) between Bragg reflections, centered at $\hbar\omega = 0$, but energetically broadened. Thereby $\hbar Q$ is the momentum transfer and $\hbar\omega$ the energy transfer during the scattering process. Protons scatter neutrons incoherently with a huge scattering cross section. Therefore in our case the quasielastic scattering

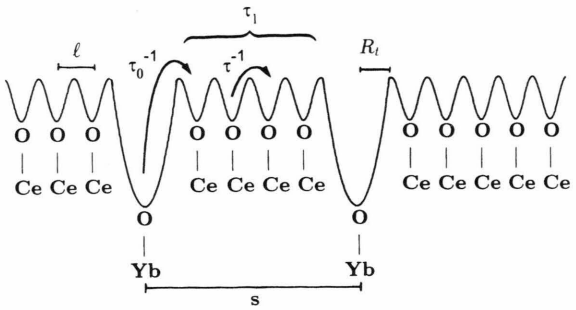

Fig. 1. Schematic view of the two state model. The temporal parameters are the jump rate τ^{-1} in the free state, the escape rate from the trap τ_0^{-1} and the trapping rate τ_1^{-1} (or the time between two trapping events τ_1). The jump length l in the free state, the distance s between two traps and the radius R_t of the trap represent the spatial parameters of this model.

intensity is proportional to the incoherent scattering function $S_i(Q, \omega)$ of the protons, which is connected via the self-part of the intermediate scattering function, $I_s(Q, t)$, to the van Hove self-correlation function, $G_s(r, t)$, by Fourier transformations in space and in time. Here the self-correlation function is the conditional probability density that, given a proton was at time $t = 0$ at the origin $r = 0$, the same proton is found at time t at the position r:

$$G_s(r,t) \xrightarrow{FT} I_s(Q,t) \xrightarrow{FT} S_i(Q,\omega)\,. \tag{1}$$

In order to formulate $G_s(r, t)$ mathematically, we first have to develop an idea about the microscopic diffusion mechanism. As we are dealing with elevated temperatures in our experiment, a classical consideration, as was done by E. Wicke for H in metals already 30 years ago [11], is fully adequate. For proton diffusion in Yb-doped $SrCeO_3$ our conception is visualized, for simplicity one-dimensionally, in Figure 1. Protons perform a random walk over the *regular proton sites*, adjacent to Ce^{4+} ions, and these sites represent local minima of the effective single particle hydrogen potential. The jump rate is τ^{-1}, the distance between two regular sites represents the jump length l. This random walk is called the *free state* of the protons, and we can define a *free diffusion coefficient*

$$D_{\text{free}} = \frac{l^2}{6\tau}\,. \tag{2}$$

At random some of the Ce^{4+} ions are substituted by Yb^{3+} ions which carry an effective negative charge and thus exert a strong Coulomb attraction on the protons. Therefore the proton site adjacent to an

Yb^{3+} ion is energetically lowered, i.e., Yb acts as a *proton trap*. In the course of its random walk, after a mean time τ_1 in the free state, a proton hits on a trap and stays there for a certain mean time τ_0 before, due to thermal fluctuations, it manages to escape again. Thus τ_1^{-1} is called the trapping rate and τ_0^{-1} the escape rate. The square of the distance between two traps, denoted by s^2, corresponds to the mean square displacement of the protons in the free state, i.e., within the time τ_1; hence

$$\frac{l^2}{6\tau} = \frac{s^2}{6\tau_1} . \tag{3}$$

For the temperature dependence of the jump rate, the trapping rate and the escape rate we assume an Arrhenius behaviour with the activation energies u, u_1, and u_0, respectively, where u and u_0 correspond to the respective barrier heights; their difference, $u_0 - u$, can be considered as the binding energy of the trap. According to the kinetics of point defects, the trapping rate is connected to the radius, R_t, the number density of the traps, N_t, and to the free diffusion coefficient [12]

$$\tau_1^{-1} = 4\pi R_t N_t D_{\text{free}} . \tag{4}$$

Therefore, since R_t and N_t are expected to be independent of temperature, the activation energies u and u_1 should be identical. This allows a check of the internal consistency of the model. The proton diffusion process thus consists of a sequence of free diffusion and trapping/escape events. The effective "long-range" self-diffusion coefficient of the protons is thereby reduced with respect to the free diffusion coefficient:

$$D_{\text{eff}} = \frac{\tau_1}{\tau_1 + \tau_0} D_{\text{free}} ; \tag{5}$$

where τ_1 is the time for free diffusion within the time unit $\tau_1 + \tau_0$.

The mathematical formulation of the self-correlation function and eventually the incoherent scattering function for a diffusion process with random traps yields a so-called *two-state-model*. Such a model was developed by Singwi and Sjölander [13] in order to understand QENS data on the proton diffusion in liquid water; Richter and Springer [14] unravelled the diffusion process of hydrogen in niobium doped with nitrogen with this kind of model; the model was extended to a three-state-model for the description of hydrogen diffusion in intermetallic compounds [15]; and the two-state-model was also used for the evaluation of QENS data on hydrogen diffusion in amorphous $Pd_{0.8}Si_{0.2}$ [16].

Details of the formalism can be found in [13]. Here we only outline the main features. The self-correlation functions. (1), of the two-state-model consists of four terms,

$$G_s(r,t) = \frac{\tau_0}{\tau_0+\tau_1} \{G_s^{tt}(r,t) + G_s^{tf}(r,t)\} + \frac{\tau_1}{\tau_0+\tau_1} \{G_s^{ft}(r,t) + G_s^{ff}(r,t)\} , \tag{6}$$

because the proton can both start and end either in the trapped or in the free state; the fractions of protons initially in the two states are given by the respective prefactors in (6). Within the time t a proton can perform 0, 1, 2, 3, ..., ∞ state transitions, hence

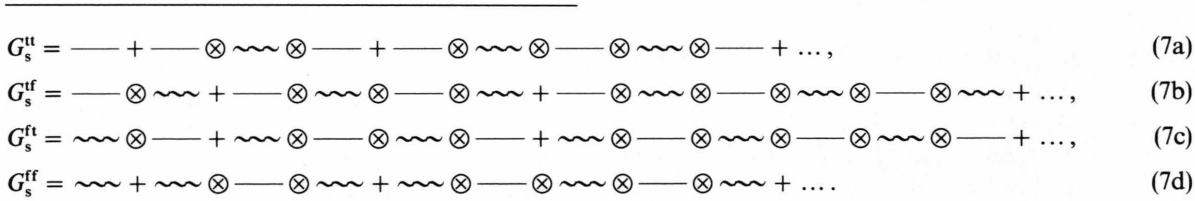

A wavy/straight line denotes the self-correlation function for the free/trapped state and ⊗ denotes the state transition. The self-correlation function for the trapped state is simply

$$G_s^t(r,t) = \exp(-t/\tau_0) \cdot \delta(r) , \tag{8}$$

whereas for the free state we insert the product of a decay function $\exp(-t/\tau_1)$ and the result of the Chudley-Elliott-model [17] for jump diffusion characterized by a jump length l and a jump rate τ^{-1}, as will be explainted later in (13). In (7) the symbol ⊗ mathematically denotes a convolution, thus $G_s(r,t)$ consists of sequences of convolutions which look very unhandy. However, by Laplace transformation $G_s(r,t)$

can be transformed into sequences of multiplications, which simply represent geometric serieses, as can be seen from

$$G_s^{tt} = \text{——} + G_s^{tf} \otimes \text{——} . \tag{9}$$

The solution in Laplace space thus turns out to be straightforward, and the result can be transcribed into the Fourier transformed of $G_s(r,t)$, the intermediate scattering function $I_s(Q,t)$ of (1). A further Fourier transformation yields the desired scattering function, which consists of a superposition of two Lorentzians:

$$S_i(Q,\omega) = \frac{w_1}{\pi}\frac{\lambda_1}{\lambda_1^2+(\hbar\omega)^2} + \frac{w_2}{\pi}\frac{\lambda_2}{\lambda_2^2+(\hbar\omega)^2}; \tag{10}$$

with the linewidths

$$\lambda_{1,2} = \frac{\hbar}{2}\left\{\tau_0^{-1}+\tau_1^{-1}+\lambda(Q) \pm \sqrt{[\tau_0^{-1}+\tau_1^{-1}+\lambda(Q)]^2 - 4\lambda(Q)\tau_0^{-1}}\right\} \tag{11}$$

and the weights

$$w_{1,2} = \frac{1}{2} \pm \frac{1}{2}\frac{\lambda(Q)\dfrac{\tau_1+\tau_0}{\tau_1+\tau_0} - \tau_0^{-1} - \tau_1^{-1}}{\sqrt{[\tau_0^{-1}+\tau_1^{-1}+\lambda(Q)]^2 - 4\lambda(Q)\tau_0^{-1}}} . \tag{12}$$

As already mentioned, for the free state a Chudley-Elliott-model is superimposed on the two-state-model; the linewidth $\lambda(Q)$ resulting from the Chudley-Elliott-model is implicitly contained in our scattering function; we use the Chudley-Elliott result for isotropic jump diffusions in liquids,

$$\lambda(Q) = \frac{1}{\tau}\left(1 - \frac{\sin Ql}{Ql}\right), \tag{13}$$

which has proved to be a very useful approximation for the (orientationally averaged) hydrogen diffusion in polycrystalline intermetallic hydrides [18].

Our scattering function, (10)–(13), thus contains the primary microscopic parameters τ_0^{-1}, τ_1^{-1}, τ^{-1}, and l; their physical meaning had been explained at the beginning of this Section. Derived quantities are s, D_{eff}, and R_t.

3. Experimental Details

The polycrystalline ceramics were prepared by solid state synthesis starting from $SrCO_3$, CeO_2 Yb_2O_3. The ceramics so obtained were gas tight and had a final density >95% of the theoretical one. Chemical analysis on the basis of atomic-emission-spectroscopy confirmed the correct composition and showed that no impurities were generated via the synthesis procedures. SEM microscopy gave a grain size distribution of 3–10 μm. X-ray diffraction ($Cu-K_\alpha$) of the pellet surfaces as well as of pulverized pellets yielded the cell parameters of the single phase material, which has a deformed perovskite structure. The unit cell is orthorhombic with the parameters: $a = 5.994$ Å, $b = 8.575$ Å, $c = 6.138$ Å, $Z = 4$.

The sample for the QENS experiment was a cylinder with 28 mm diameter and 30 mm height (approx. 110 g); it was charged with protons at 600 °C for 120 h in a gas flow system (21 vol% O_2 in Ar with a water vapour partial pressure of 50 mbar). Maintaining wet atmosphere, the sample was sealed in a platinum sample holder by welding. The QENS experiment was performed at the ISIS pulsed neutron source of the Rutherford Appleton Laboratory. We used the reverse geometry time-of-flight backscattering spectrometer IRIS [19]: a white beam, limited to 9 Å $< \lambda <$ 11 Å by disk choppers in the incident beam, falls on the sample, the scattered neutrons being analyzed by means of mica (004) crystals almost under backscattering condition at $\lambda = 9.9$ Å. This setting of the spectrometer gives an energy resolution of 4.2 μeV FWHM over an energy transfer range of ±80 μeV. Quasielastic spectra were recorded in 51 different scattering angles between 20° and 140° which are binned into six groups corresponding to Q values between 0.29 $Å^{-1}$ and 1.21 $Å^{-1}$ at room temperature (used as resolution function) and at 5 different temperatures between 673 K and 1073 K. At room temperature an empty Pt can was measured for the background subtraction.

The impedance spectra (IS) were recorded in-situ between room temperature and 1273 K to determine the total bulk conductivity. The pellets with a diameter of 14 or 23 mm and a thickness of 1 mm maximum were covered with porous platinum electrodes. The frequency range was between 10^{-2} and 10^7 Hz and the a.c. excitation voltage 10 mV. Also potential difference measurements in a steam concentration cell were performed in order to separate the protonic conductivity contribution from the electronic conduction.

4. Results

4.1 Model-Independent Scattering Results

Figure 2 displays some of our neutron scattering spectra; a broadening of the spectra with increasing

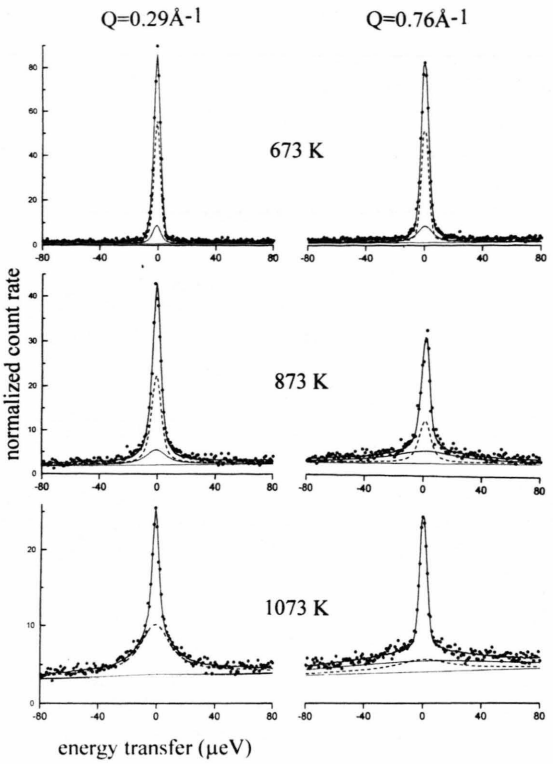

Fig. 2. Neutron scattering spectra for three temperatures at the momentum transfers $Q=0.29$ Å^{-1} and $Q=0.76$ Å^{-1}. The solid lines show the total scattering function resulting from the final fit with the two state model as well as the flat background. The dotted and broken lines represent, respectively, the first and the second Lorentzian due to (10).

temperature is clearly visible and indicates proton diffusivity. Also with increasing momentum transfer the spectra become broader. The Q dependence of the spectra bears information about the spatial extension of the diffusive process.

On closer inspection we notice that the spectra consist of several scattering contributions. One of them is the elastic scattering due to the host lattice, since the background subtraction was done only with an empty Pt can. The main constituents have a zero ($\sigma_i^{Ce} = \sigma_i^0 = 0.00$ barn [20]) or nearly zero ($\sigma_i^{Sr} = 0.04$ barn) incoherent neutron scattering cross section, and Yb ($\sigma_i^{Yb} = 3.0$ barn) is present only in low concentration. Therefore the incoherent elastic scattering of the host is very small (0.19 barn per formula unit). But, there is some Laue scattering [21] due to the random distribution of Yb and Ce on the Ce sublattice; hence the elastic scattering contribution of the host lattice is given by

$$4\pi\left(\frac{d\sigma}{d\Omega}\right)_{host} = \sum_n \nu_n \sigma_i^n + 4\pi x(1-x)(b_{Yb}-b_{Ce})^2 + (0.19+0.34)\text{ barn}, \quad (14)$$

where the differential scattering cross section is per formula unit, ν_n denote the stoichiometric factors and x is the atomic fraction of Yb on the Ce sublattice. The elastic scattering amounts to about a quarter of the total scattering (disregarding the flat background).

A further notable feature of the spectra in Fig. 2 is the flat background which increases strongly with increasing temperature. The reason for this background is unclear at present. It could be an artefact of the spectrometer: the furnace used for the experiment to some extent also warms up the mica analyzer crystals of the spectrometer and thus possibly stimulates incoherent mica scattering due to some residual hydrogen/water content. It could be due to the (weighted) phonon density of states of the host lattice: with increasing temperature more and more phonons are created. But it could also be due to the protons in our sample or in the surrounding atmosphere.

A fit of the spectra with an elastic contribution and one Lorentzian turned out to be inadequate, and therefore we performed fits with an elastic contribution and two Lorentzians. A comparison of the fits is shown in Fig. 3; the difference is particularly visible in the residuals: for the one-Lorentzian-fit the residuals exhibit a certain "structure" whereas for the two-Lorentzian-fit they are distributed at random. Therefore we individually fitted all of our spectra with two Lorentzians, an elastic contribution and a flat background in order to get some insight into the diffusion mechanism unbiased by any model; fits of this kind with such a large number of variables, however, are delicate; the results can at most be considered as semi-quantitative; these model-independent fits should, however, unravel the trends and direct us to an appropriate model, see Section 4.2. For one particular Q value, $Q=0.95$ Å^{-1}, Fig. 4 displays the temperature dependence of the widths of the broad and narrow lines resulting from the two-Lorentzian fits of the spectra. It shows an Arrhenius behaviour; the activation energy of the narrow component is considerably larger than that of the broad component. This result clearly indicates that energetically different proton sites exist in $SrCe_{0.95}Yb_{0.05}H_{0.02}O_{2.985}$ and that the proton diffusion process comprises different proton

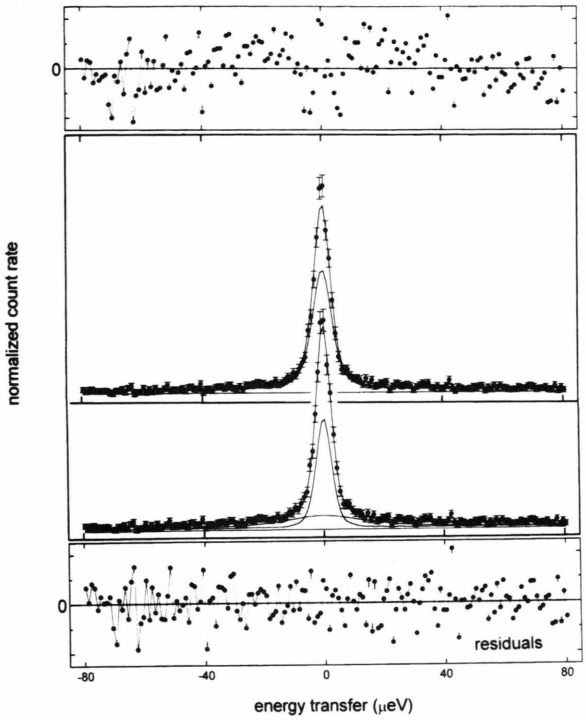

Fig. 3. Comparison between a model independent fit with a scattering function consisting of one Lorentzian (upper part) and two Lorentzians (lower part) for $T=500\,^{\circ}\mathrm{C}$ and $Q=1.21\ \text{Å}^{-1}$. The residuals as the difference between experiment and theory, weighted with the measurement error, show in the first case a systematic deviation while in the second, they are statistically distributed emphasizing the good quality of the fit.

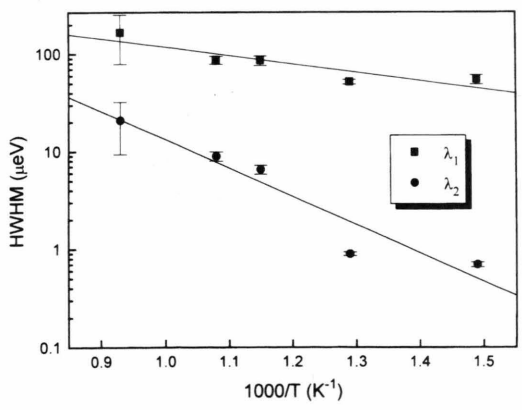

Fig. 4. Temperature dependence of the linewidths of the two Lorentzians at $Q=0.95\ \text{Å}^{-1}$. The activation energies differ considerably which indicates energetically different proton sites.

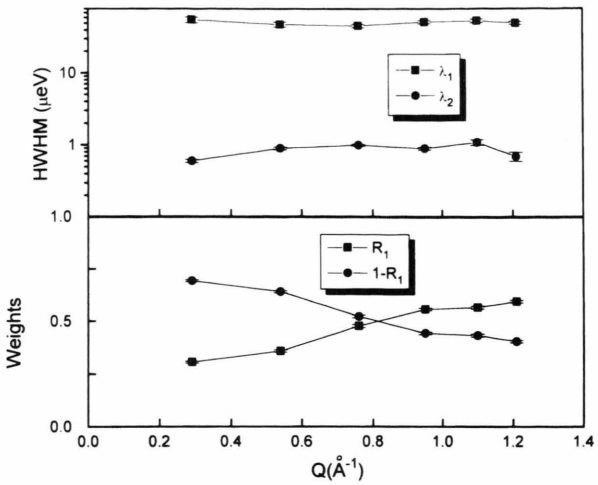

Fig. 5. Q-dependence of the linewidths and the weights of the two Lorentzians forming the scattering function as a result of the model independent data analysis at $T=773$ K. This behaviour is typical for a two state model (see Figure 6).

jumps. For a particular temperature, $T=773$ K, Fig. 5 displays the Q dependence of the line widths (upper part of the figure) and of the weights (lower part). Even at our smallest Q value, $Q=0.29\ \text{Å}^{-1}$, we are not in the validity regime of the so-called Q^2 law which states that for any diffusion process at sufficiently small Q the scattering function consists of a single Lorentzian with a linewidth $\lambda=\hbar D_s Q^2$, whereas we clearly observe two Lorentzians and no Q^2 dependence. Therefore from our model-independent data evaluation it is not possible to extract the self-diffusion coefficient of the protons. The Q dependences in Fig. 5, however, remarkably resemble the corresponding Q dependences of the two-state-model introduced in Sect. 2 (for a comparison see Figure 6). Together with the temperature dependences of Fig. 4 this motivates us to apply the two-state model to our data.

4.2 Evaluation of the Scattering Data in the Framework of the Two-State-Model

The scattering function of the two state model is given in (10)–(13). In order to avoid statistical fluctuations it turned out to be necessary to combine all spectra (5 temperatures, 6 Q values, i.e., 30 spectra) into one set of data and fit the ω, Q, and T dependences simultaneously. Thereby for the temperature dependence of the different rates we made a respective Arrhenius ansatz, and for the Q dependence of the

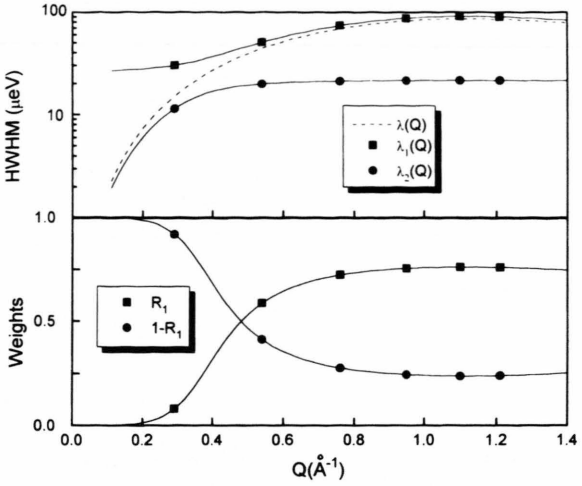

Fig. 6. Q-dependence of the linewidths and weights of the two Lorentzians forming the scattering function of the two state model shown for $T=1073$ K. These values are a result from a global fit of 5 temperatures and 6 Q-values per temperature.

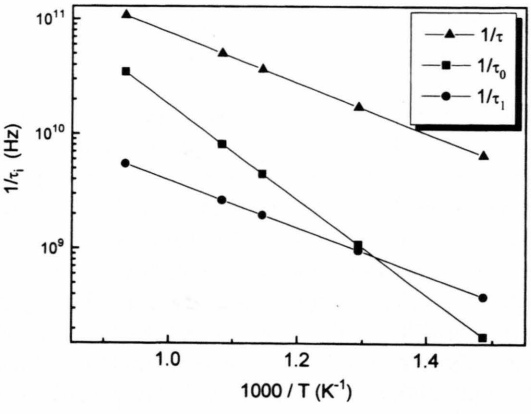

Fig. 7. Temperature dependence of the escape rate τ_0^{-1}, trapping rate τ_1^{-1} and jump rate τ^{-1}.

(hypothetical) undisturbed free diffusion the ansatz (13). The parameters of the model common to all spectra thus are the three prefactors and three activation energies of the rates τ^{-1}, τ_0^{-1}, and τ_1^{-1} and the jump length l as well as the relative intensity of the elastic contribution. The flat background turned out to be independent of Q, but variable with respect to temperature. In order to stabilize the fit, the quasielastic to elastic intensity ratio was taken as a temperature independent common fitting parameter, although we are aware of the fact that with increasing temperature some hydrogen (in the form of water molecules) is desorbed which would change the intensity ratio. But firstly the sample is sealed in the platinum container and the desorbed water increases the water vapour pressure, and secondly, even with constant outer water vapour pressure, the H concentration change between 600 °C and 800 °C only amounts to about 10% of the total H content [5]. For the purpose of our data evaluation we consider the change of the H content as negligible. The finally resulting scattering function is displayed as solid lines in Figure 2. For a particular temperature $T=1073$ K, Fig. 6 displays the Q dependences of the line widths and weights for this scattering function. The full squares and circles indicate the Q values where data had been taken.

In this way we obtain the following results:

$$\tau_0^{-1} = (2.6 \pm 1.9) 10^{14} \exp\{-(824 \pm 57)\,\text{meV/kT}\}\,\text{s}^{-1},$$

$$\tau_1^{-1} = (4.8 \pm 4.7) 10^{11} \exp\{-(413 \pm 73)\,\text{meV/kT}\}\,\text{s}^{-1},$$

$$\tau^{-1} = (1.2 \pm 0.4) 10^{13} \exp\{-(436 \pm 21)\,\text{meV/kT}\}\,\text{s}^{-1},$$

$$l = 4.0 \pm 0.2\ \text{Å}.$$

The temperature dependences of the rates are graphically represented in Figure 7. The effective (long range) self-diffusion coefficient D_{eff} was calculated for each of our temperatures by means of (5) and is displayed as squares in the Arrhenius plot of Figure 10. Since it is obtained as a superposition of Arrhenius functions, D_{eff} itself does not obey the Arrhenius law. However, within our limited temperature range 673 K to 1073 K, it can be represented by this function in good approximation:

$$D_{\text{eff}} = 19.5 \cdot 10^{-3} \exp(-605\ \text{meV/kT})\,\text{cm}^2\,\text{s}^{-1}.$$

From the jump length l and the ratio of jump rate and trapping rate by means of (3) we obtain the mean square displacement, s^2, of the protons in the free state and thus the average distance, $s=17$ Å, between two traps. From the ratio of the quasielastic scattering intensity (due to H) and the elastic scattering intensity (due to the host lattice) we deduce a hydrogen concentration of 1.95 mol% in the sample which is in agreement with the value of 2 mol% from the chemical sample preparation.

4.3 Electrochemical Results

The conductivity has electronic and protonic contributions. These were unravelled in an electrochemical hydrogen concentration cell [22]. Generally, if in a

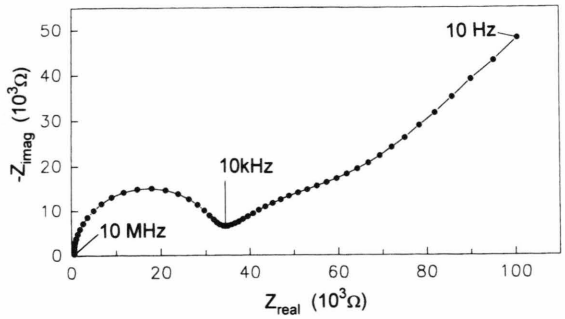

Fig. 8. Impedance spectrum at 473 K of the ceramic in the form of a Nyquist plot. Going from high to low frequencies, one distinguishes contributions from the bulk, the grain boundaries and the electrode.

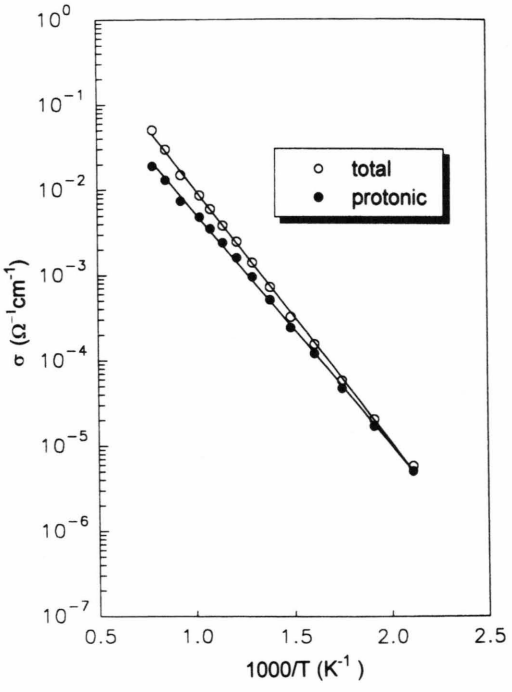

Fig. 9. Total conductivity and protonic conductivity in an Arrhenius representation. At higher temperatures, the protonic fraction of the conductivity decreases. This is in agreement with the fact, that this material behaves like a semi-conductor, so that the electronic conductivity becomes more important at higher temperatures.

galvanic cell the solid electrolyte exhibits also partial electronic conductivity, the measured open-circuit voltage in a concentration cell is, due to the inner short-cut, reduced with respect to the Nernst value to the extent of the electronic contribution. The thus obtained transport numbers decrease linearly with in-

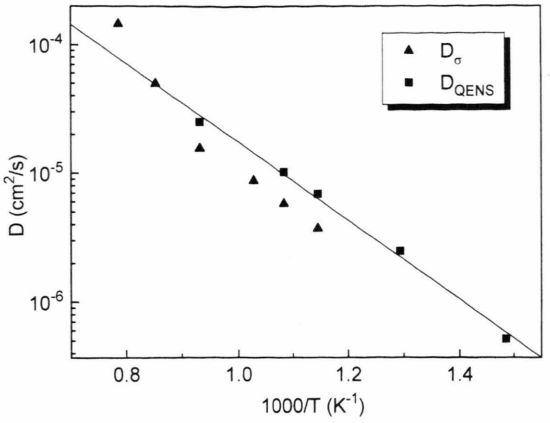

Fig. 10. Self diffusion coefficient D_{QENS} obtained from QENS compared to the conductivity diffusion coefficient D_σ from IS. The solid line represents the Arrhenius fit of the D_{QENS} values.

creasing temperature from $t_H = 0.9$ at 473 K to $t_H = 0.4$ at 1273 K. A typical impedance spectrum is shown in Figure 8. Going from high to low frequencies it is possible to distinguish the semicircles ascribed to bulk, to grain boundaries diffusion and to the platinum/cerate electrode interface contributions. Increasing the temperature leads to a shift of the spectra in the direction of higher frequencies and lower impedance values. At temperatures above 673 K the grain boundary semicircle is no longer distinguishable. From a computer fit [23] of the ohmic resistance at high frequencies and the geometry of the specimen the specific bulk conductivity is calculated (upper curve in Figure 9). Multiplying these conductivities with the transport numbers yields the protonic part σ_p of the bulk conductivity (lower curve in Figure 9). This correction of the conductivity data obtained by the impedance spectroscopy is most evident at higher temperatures due to the increasing electronic (semi-)conductivity contribution. The activation energy of the protonic conductivity amounts to 610 meV.

From the impedance results the conductivity diffusion coefficient of the proton is obtained by applying the Nernst-Einstein-relation

$$D_\sigma = \frac{\sigma_p k T}{N_H e_0^2}; \tag{15}$$

k, T and e_0 have their usual meaning. N_H is the hydrogen (proton) number density, for which we used the values reported by Iwahara [5]. In general, the thus obtained conductivity diffusion coefficient is different

from the self-diffusion coefficient measured by QENS; at vanishing concentration, however, the different diffusion coefficients coincide. Therefore, a comparison of both our diffusion coefficients, as shown in an Arrhenius representation in Fig. 10, is immediately possible.

5. Discussion

The present study clearly demonstrates that by means of QENS it is possible to observe the proton diffusion and thus the proton conductivity process in a high temperature proton conductor on an atomistic scale simultaneously of space and time. In the proton conducting prevoskite $SrCe_{0.95}Yb_{0.05}H_{0.02}O_{2.985}$ – this was not clear prior to our study – the lattice sites visited by the proton in the course of the diffusive process are energetically non-equivalent. Thus the proton diffusion is complex and consists of a sequence of free diffusion and trapping/escape events. QENS proves the existence of so-called traps which immobilize the protons for some time, but QENS by itself is not able to identify these traps. However, we can correlate our resulting spatial parameters to typical distances in the structure of the investigated perovskite:

mean jump length $l = 4.0$ Å $\leftrightarrow$ mean distance $d_{O-O} = 3.2$ Å,
mean distance between traps $s = 17$ Å $\leftrightarrow$ mean distance $d_{Yb-Yb} = 12$ Å,
trap radius $R_t = 2.6$ Å $\leftrightarrow$ mean distance $d_{Ce-O} = 2.3$ Å.

d_{O-O} and d_{Ce-O} originate from crystallographic data [24], d_{Yb-Yb} was estimated from the Yb^{3+}-concentration, and the trap radius R_t was calculated, identifying the Yb^{3+}-concentration with the trap concentration N_t from (4). We consider the agreement as reasonable and therefore tentatively conclude: i) in the free state the protons jump from oxygen to oxygen ions, ii) after about 20 jumps in free state (ratio τ_1/τ) trapping occurs at Yb^{3+} ions. The binding energy of the trap turned out to be 388 meV (= difference of the activation energies of the escape and jump rates).

We obtained the same values within the limits of error for the activation energies of the jump rate and the trapping rate, both independently variable in the final fits. We consider this as confirmation of the internal consistency of our two state model because according to (4) both quantities have to be identical if the product of the trap radius and the trap concentration is independent of temperature. The validity of our data evaluation procedure is also supported by the fact that the ratio between the quasielastic scattering intensity due to the migrating protons and the elastic scattering which is attributed to the immobile host yields the correct hydrogen content of our sample.

The free state and the trapped state of the protons are populated according to the Boltzmann factor, and therefore at room temperature or at lower temperatures essentially all protons should occupy a trap site, i.e., a site adjacent to an Yb^{3+} ion. This is in agreement with Yugami et al. [25] who by optical methods (UV spectroscopy) have measured crystal field transitions of Eu^{3+} and Pr^{3+} ions in Eu_2O_3- or Pr_2O_3-doped $SrCeO_3$ and found that protons, introduced into these compounds, are located in the immediate vicinity of the Eu^{3+} or Pr^{3+} ions, respectively.

We still have problems with the flat background in our spectra: it is strongly temperature dependent and obeys an Arrhenius law remarkably well. It could represent a broad quasielastic component which within the limited energy window of the applied spectrometer is not detectable. A broad quasielastic component means a fast motion. Up to now it is not clear whether this fast localized motion, if it exists, is somehow connected to the diffusion process (perhaps a localized motion within the trap) or whether it possibly represents a proton motion for instance in grain boundaries.

Finally, Fig. 10 compares the effective self-diffusion coefficient from QENS calculated in the framework of the two-state model with the conductivity diffusion coefficient from IS. The agreement is remarkable, in particular the activation energies are practically identical within the temperature range of the QENS experiment. This agreement strongly supports our model. The slight ratio of 1.7 on average between the prefactors could be due to uncertainties in the carrier concentration, which enters into the Nernst-Einstein equation.

6. Conclusion

With this first quasielastic neutron scattering experiment on a proton conducting oxide we have demonstrated that QENS is able to elucidate the microscopic proton diffusion mechanism and thus helps to fundamentally understand the proton conductivity mechanism in this class of materials. The sample was polycrystalline; single crystalline samples considerably enhance the power of QENS and would be most desirable. Some questions are still open, and further QENS investigations are already in progress.

Acknowledgement

We thank U. Stimming (KFA Jülich) for valuable discussions and M. A. Adams (RAL) for his help during the experiment; financial support of R. H. by the *Fonds der Chemischen Industrie* is gratefully acknowledged.

[1] T. Norby, Solid State Ionics **40/41,** 857 (1990).
[2] H. Iwahara, Solid State Ionics **28–30,** 573 (1988).
[3] H. Iwahara, H. Uchida, K. Ono, and K. Ogaki, J. Electrochem. Soc. **135,** 529 (1988). D. A. Stevenson, N. Jiang, R. M. Buchanan, and F. E. G. Henn, Solid State Ionics **62,** 279 (1993).
[4] H. H. Huang and M. Ishigame, Solid State Ionics **47,** 251 (1991).
[5] H. Iwahara, High temperature proton conductors based on perovskite-type oxides, in: P. Colomban (Ed.), Proton Conductors, Cambridge University Press, 1992.
[6] H. Iwahara, Proceedings of the International Conference on Solid State Proton Conductors VII, Schwäbisch Gmünd 1994, to be published in Solid State Ionics.
[7] preliminary results were presented at the International Conference on Solid State Proton Conductors VII, Schwäbisch Gmünd 1994: R. Hempelmann, Ch. Karmonik, Th. Matzke, M. Cappadonia, U. Stimming, T. Springer, and M. A. Adams, Solid State Ionics, in print.
[8] H. Uchida, N. Maeda, and H. Iwahara, Solid State Ionics **11,** 117 (1983).
[9] T. Springer, Quasielastic Neutron Scattering for the Investigation of Diffusive Motions in Solids and Liquids, Springer Tracts in Modern Physics, Vol. **64,** Springer, Berlin 1972.
[10] M. Bée, Quasielastic Neutron Scattering, Adam Hilger, Bristol 1988.
[11] E. Wicke, Proceedings of Simposio Dinamica delle Razioni Chimiche, Padova 1966.
[12] R. Waite, Phys. Rev. **107,** 471 (1957).
[13] K. S. Singwi and A. Sjölander, Phys. Rev. **119,** 863 (1960).
[14] D. Richter and T. Springer, Phys. Rev. B **18,** 126 (1978).
[15] R. Hempelmann, J. Less-Common Metals **101,** 69 (1984).
[16] D. Richter, G. Driesen, R. Hempelmann, and I. S. Anderson, Phys. Rev. Lett. **57,** 731 (1986).
[17] T. Chudley and R. J. Elliott, Proc. Phys. Soc. London **77,** 353 (1961).
[18] D. Richter, R. Hempelmann, and L. A. Vinhas, J. Less-Common Metals **88,** 353 (1982).
[19] C. J. Carlile and M. A. Adams, Physica B **182,** 431 (1992).
[20] V. F. Sears, Neutron Scattering Lengths and Cross Sections, in: D. L. Price and K. Sköld (Eds.), Methods of Experimental Physics Vol. 23 A, Academic Press, San Diego 1987.
[21] W. Schmatz, Disordered Structures, in: H. Dachs (Ed.), Neutron Diffraction, Topics in Current Physics Vol. 6, Springer, Berlin 1978.
[22] T. Norby, Solid State Ionics **28–30,** 1586 (1988).
[23] B. A. Boukamp, Equivalent Circuit, Internal Report CT 89/214/128, University of Twente (The Netherlands), 1989.
[24] A. Saiki, Y. Seto, H. Seki, H. Ishizawa, and M. Kato, Nippon Kagaku Kaishi **1,** 25 (1991).
[25] H. Yugami, S. Matsuo, Y. Chiba, and M. Ishigame, Proceedings of the International Conference on Solid State Proton Conductors VII, Schwäbisch Gmünd 1994, to be published in Solid State Ionics.